Original Article

SHM Structural Health Monitoring

Structural Health Monitoring
2017, Vol. 16(6) 663–673

DOI: 10.1177/1475921716678921
journals.sagepub.com/home/shm
SAGE

Barely visible impact damage imaging using non-contact air-coupled transducer/laser Doppler vibrometer system

MS Harb[1] and FG Yuan[2,3]

Abstract

The aim of this study is to investigate the capability of the zero-lag cross-correlation imaging condition of an A_0 Lamb wave mode in imaging a barely visible impact damage in a carbon fiber–reinforced polymer composite using a fully non-contact-guided wave-based non-destructive inspection system. A 16-ply $(45/0/\text{-}45/90)_{2s}$ carbon fiber–reinforced polymer laminate was impacted at three different locations with different impact energies using a drop ball at three drop heights causing three barely visible impact damages with different sizes. The A_0 Lamb wave mode is generated inside the laminate using a circular air-coupled transducer and detected along the damaged region using a laser Doppler vibrometer. The measured wavefield is then decomposed into a forward and backward propagating wavefields by applying a frequency–wavenumber filtering post-processing technique. The decomposed wavefields are then cross-correlated in the frequency domain using zero-lag cross-correlation imaging condition producing a detailed cumulative damage image. The images obtained in frequency domain highlight the three damaged areas with higher zero-lag cross-correlation values compared to other parts of the inspected areas. The experimental investigation has shown a good correlation between the zero-lag cross-correlation imaging condition and C-scan images, which demonstrate a strong capability of guided wave zero-lag cross-correlation imaging condition technique in approximating the location and size of relatively small barely visible impact damages in thin composite structures.

Keywords

Lamb waves, barely visible impact damage, delamination, composite, zero-lag cross-correlation imaging condition, non-destructive inspection

Introduction

Many contact and non-contact non-destructive inspection (NDI) techniques have been extensively investigated to fulfill the need for rapid, autonomous, and effective ways to evaluate and monitor the health of an aerospace structure to ensure its safety and predict its remaining useful life.[1,2] Among the non-contact NDI techniques, interferometers and laser Doppler vibrometers (LDV) are considered effective sensors for Lamb wave measurements of a plate due to their superior sensitivity and the direct focus of the laser beam at a point of interest on the inspected surface and thus overcoming the energy dissipation between media when Lamb waves are measured using water coupled, wedge, or air-coupled transducers (ACTs). Single-point or one-dimensional (1D) vibrometers are among the commonly used vibrometers in the NDI which can measure one-directional out-of-plane movement. The 1D LDV used for the dynamic visualization Lamb waves in a plate will mostly detect the modes with the dominant out-of-plane vibrations known as anti-symmetric (A) modes.

[1]Department of Mechanical Engineering, American University of Beirut, Beirut, Lebanon
[2]Department of Mechanical and Aerospace Engineering, North Carolina State University, Raleigh, NC, USA
[3]Integrated Structural Health Management Laboratory, National Institute of Aerospace, Hampton, VA, USA

Corresponding author:
FG Yuan, Department of Mechanical and Aerospace Engineering, North Carolina State University, 911 Oval Drive-3306 EBIII, Campus Box 7910, Raleigh, NC 27695, USA.
Email: yuan@ncsu.edu

The propagation and characterization of Lamb waves have been intensively studied and used for damage detection in metallic and composite structures. Specifically, the interaction of the fundamental symmetric (S) and anti-symmetric (A) modes with different types of damages has been previously investigated to better understand the behavior of Lamb waves in damaged structures, that is, reduction in amplitude, change in time-of-flight (TOF), mode conversion, and backscattered waves which would simplify the wave analysis and lead to better damage detection and imaging. Kazys et al.[3] investigated numerically and experimentally the scattering of Lamb wave from an artificial delamination in a honeycomb composite by measuring the signals generated right above the inhomogeneities using a complete air-coupled non-contact method. A strong wave leakage was detected over the damaged area that was estimated when the amplitudes were plotted as a C-scan image. The same research group obtained similar results when testing square-shaped carbon fiber–reinforced polymer (CFRP) composite rods for defects.[4] A study by Ramadas et al.[5] was done to numerically and experimentally detect two artificial delaminations of 40 and 50 mm in length in glass-fiber reinforced plastic (GFRP) using TOF of A_0 Lamb wave mode generated and measured using ACTs in a pitch-catch mode and showed a close prediction of the actual damage size. In another work, Ramadas et al.[6] studied the interaction of A_0 mode with structural discontinuity in a more complex composite, glass/epoxy T-joint. It was found that an S_0 mode is formed from the propagating A_0 due to the presence of a discontinuity (spar web) where its location could be determined using TOF of both modes.

However, in the case of air-coupled generation and detection of Lamb waves, different experimental errors could be easily realized within the measured data. The high impedance mismatch between air and inspected medium causes a huge loss in energy at the interface, which makes damage detection using change of propagating Lamb wave amplitude harder and less efficient. The excitation and reception regions by the ACT are large when compared to a contact Lead Zirconate Titanate (PZT) or laser pulse, which makes the TOF or change of velocity techniques for possible presence of defects also insufficient. The authors recently have demonstrated the use of the non-contact ACT/LDV system for measuring the dispersion curve characterization[7] and damage imaging of damaged aluminum plates.[8]

Therefore, the objective of this study is to investigate the detection and imaging of barely visible impact damages (BVIDs) in a composite laminate using a fully non-contact ultrasonic technique without a priori knowledge of the material characteristics, composite layup, damage size, location, and any baseline data. The investigation is held based on the interaction of an A_0 Lamb wave mode with different delaminations and the cross-correlation between the forward propagating wavefield and the backward propagating wavefield formed due to the wave interaction with the damage.

Section "Theoretical background" presents a short background and description of the frequency–wavenumber filtering method used for decomposing the generated Lamb wavefield and the zero-lag cross-correlation (ZLCC) imaging condition technique. Section "Non-contact experimental verification" presents a detailed explanation of the experimental configuration and setup, the composite material used, and the damaged areas; it presents the experimental imaging results for three different damages compared with traditional C-scan images and finally discusses the feasibility of the proposed system, and filtering and imaging technique in visualizing BVIDs. Finally, the conclusions are discussed in section "Conclusion."

Theoretical background

The raw data collected by the scanning system contain information about the interior of the inspected structure and could be studied in depth to characterize the health of the structure. A propagating wave inside a plate-like structure could be easily seen by displaying the recorded data in three-dimensional (3D) space, two axes representing the scanning area (x and y), and the third is the time (t) axis. As shown in Figure 1, an incident Lamb wave propagating along the thickness of the plate that interacts with damage is partially reflected and the rest is transmitted through.

In order to understand and clearly see the backscattered waves from the damage, the recorded Lamb wave is decomposed into incident (forward) and reflected backscattered (backward) waves, propagating along the plate in the positive and negative x directions, respectively, as seen in Figure 1. This separation is done using a simple fast frequency–wavenumber filtering technique, which was proposed by Ruzzene[9] for the visualization of damage reflections in plate structures and later was used for the characterization of guided wavefields as well as detection, localization, and quantification of structural damage by Michaels et al.[10] In addition, it has been applied previously for the analysis of multi-mode Lamb wave signal processing at high frequencies for the characterization of dispersion relations and the separation of various modes.[11] Tian and Yu[12] have also analyzed Lamb waves and its propagation characteristics using frequency–wavenumber filtering and advanced wavenumber analysis as well as space–frequency–wavenumber analysis for crack detection in an aluminum plate.[13]

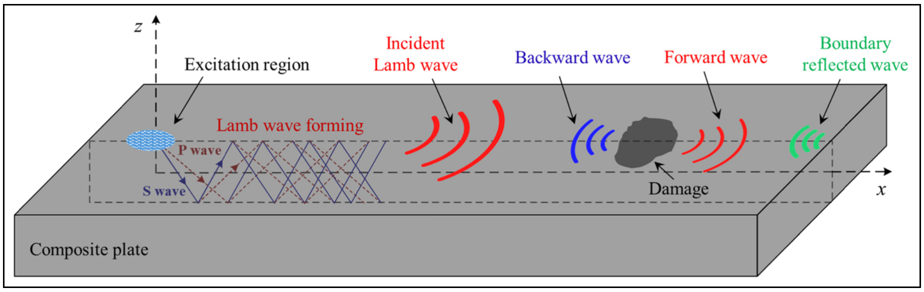

Figure 1. Schematic diagram of Lamb wave formation and propagation in a composite plate and its interaction with damage.

In this study, the frequency–wavenumber filtering technique is applied in the case of 3D domain (x, y, t). A 3D data matrix is obtained from an area scan on the inspected plate. The captured propagating wave has a wavefield $v(x, y, t)$ in terms of the time variable t and spatial variables x and y. Each data point is individually transformed into $V(k_x, k_y, \omega)$ domain by applying the 3D temporal and spatial Fourier transform with respect to x, y, and t and is expressed as follows

$$V\left(k_x, k_y, \omega\right) = FFT_{3D}(v(x, y, t)) = \int_{-\infty}^{+\infty}\int_{-\infty}^{+\infty}\int_{-\infty}^{+\infty} v(x, y, t)e^{-i\left(k_x x + k_y y - \omega t\right)}dxdydt \quad (1)$$

and the inverse Fourier transform of equation (3) gives

$$v(x, y, t) = FFT_{3D}^{-1}\left(V\left(k_x, k_y, \omega\right)\right) = \frac{1}{8\pi^3}\int_{-\infty}^{+\infty}\int_{-\infty}^{+\infty}\int_{-\infty}^{+\infty} V\left(k_x, k_y, \omega\right)e^{i\left(k_x x + k_y y - \omega t\right)}dk_x dk_y d\omega \quad (2)$$

Different signal processing methods have been previously proposed for the detection and imaging of damages in isotropic and anisotropic structures including wave energy trapping and localization,[14] wavelet-transformed ultrasonic propagation imaging,[15] standing waves,[16] cumulative total wave energy (CTWE), and cumulative standing wave energy (CSWE).[17] Time-reversal is also another technique that has been successfully used in structural health monitoring (SHM) for quantitative imaging of damage; however, when implemented in time domain it is very time-consuming. Thus, time-reversal technique has been studied in frequency–wavenumber domain for fast detection of damages in plate-like structures using flexural plate waves and cross-correlation imaging condition in the frequency domain, and damage images were obtained.[18] The key idea by which the imaging condition is defined is based on the concept that damage exists at places where forward propagating wavefield and backward propagating wavefield are in phase.

A conventional cross-correlation imaging condition based on the reconstructed wavefields can be formulated in the time (t) or frequency (ω) domain as the zero-lag of the cross-correlation between a "source" wavefield (W_s) and a "receiver" wavefields (W_r).[19] This method was first illustrated and applied in the context of reverse-time migration by Chang and McMechan,[20] which is a generalization of time-coincidence imaging condition by Claerbout.[21] In the case of SHM and NDI, the "source" wavefield originates as the forward wavefield (W_F) propagating in the medium prior to any interaction with discontinuities, and the "receiver" wavefield originates as the backward propagating wavefield (W_B) from any damages or structural boundaries. In this study, cross-correlation imaging condition is employed in the frequency domain, and the image of the inspected area is visualized by taking the ZLCC value of the two former wavefields at all scanned points as follows

$$I(x, y) = \sum_{\omega} W_F(x, y, \omega)W_B^*(x, y, \omega) \quad (3)$$

where $I\ (x, y)$ is the ZLCC value at point (x, y). The subscripts "F" and "B" represent the forward and backward wavefields, respectively, and the superscript "*" symbolizes the complex conjugation. The two wavefields kinematically coincide at the discontinuities, and the value I will be relatively large at the damage domain compared to the pristine region where it will be small or near zero and can be visualized by plotting the discrete values of I in a contour map.

Non-contact experimental verification

Experimental setup

The ACT/LDV system constitutes a non-contact air-coupled ultrasonic transducer (ACT), a Tektronix 3022B function generator, a Krohn-Hite 7602 wide-band amplifier, an IAI bi-axial translation stage and a rotary stage, a Polytec vibrometer with velocity decoder and data management system, and a computer for

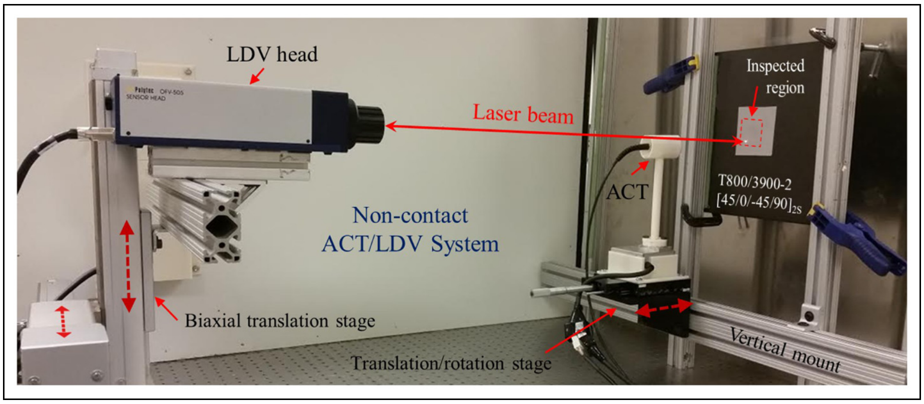

Figure 2. Actual experimental setup for damage imaging in a composite plate.

hardware control and signal processing. IAI: Intelligent Actuator, Inc.

The experimental setup is shown in Figure 2. A 200-kHz center frequency ACT with 25 mm active diameter, provided by Ultran Group, USA, is held by a 3D printed fixture and mounted on an IAI motorized rotary stage that finely controls the orientation angle with an angular resolution of 0.01°. The ACT is oriented at 14°, which was found experimentally to give the highest amplitude for the A_0 mode of interest.[7,22] The generated ultrasonic wave propagates along the 0° direction with respect to the fiber orientation. Using Snell's law, it is found that the phase velocity (c_p) of propagating A_0 mode along the 0° is ~1420 m/s, and the wavelength (λ) is 7.09 mm for the given excitation signal. The separation distance between the ACT front membrane and the inspected plate is fixed at approximately 80 mm. The inspected plate is vertically placed on a vertical mount on an optical table.

The LDV is a single-point vibrometer (Polytec OFV-500) placed on the IAI bi-axial translation stage, which measures the wave velocity component in the direction of the laser beam determined based on the Doppler phase-shift effect on light waves. It measures the out-of-plane velocity in the range of 0.01–10 μm/s over the target surface. The bi-axial translation stage can maneuver the LDV head rapidly within a two-dimensional scan field. The LDV scans horizontally to the right, step vertically upward, and then scans horizontally to the left, and the distance between the front lens of the LDV and the plate is fixed at approximately 642 mm for ultimate laser beam focusing, which is found using a *laser-target distance* equation recommended by the manufacturer. The shortest distance between the inspected scanned region and the center of the excited region is kept at approximately 75 mm. In order to improve the captured signal quality and thus increase the signal-to-noise ratio, a retroreflective tape is applied to the area to be scanned which enhances the surface reflection, in addition to the measurement at each scanned point was averaged 25 times.

The scanning speed is dependent on the LDV and ACT used, the data management system, number of averaged signals per scanned point, and the bi-axial translation stage. With the current devices and setup used, the scanning rate of inspection was fixed at 1.5 s per scanning point with a 25 averaging cycle. Thus, a 35 mm × 35 mm scanning area with a 1-mm resolution (1225 scanned points) is normally scanned in approximately 30 min which is relatively slow when compared to an air-coupled or water coupled C-scanning ultrasound inspection. However, the ACT/LDV system presented here could be optimized with the use of better and much faster translation stage that is more stable, a more advanced acquisition system, and less averaging cycles where the aforementioned area could be scanned in less than a minute.

The composite material used in this study is T800/3900-2 carbon/epoxy. One laminate $(45/0/-45/90)_{2s}$ is prepared for all the tests with the following dimensions 304 mm × 304 mm × 2.4 mm. The laminate was then impacted using a drop ball impactor at three different locations as shown in Figure 3 at three different drop heights causing BVIDs. The defects shown in Figure 3 represented by Damage I, Damage II, and Damage III were made by impact energies of 14, 19, and 27 J, respectively, and the damaged areas were then C-scanned.

The input excitation signal applied to the ACT is a narrowband, five-cycle Hanning-windowed toneburst with 200 kHz center frequency generated by the Tektronix function generator and governed by

$$V(t) = S\left(H(t) - H\left(t - \frac{N}{f_c}\right)\right)\left(1 - \cos\frac{2\pi f_c t}{N}\right)\sin(2\pi f_c t) \tag{4}$$

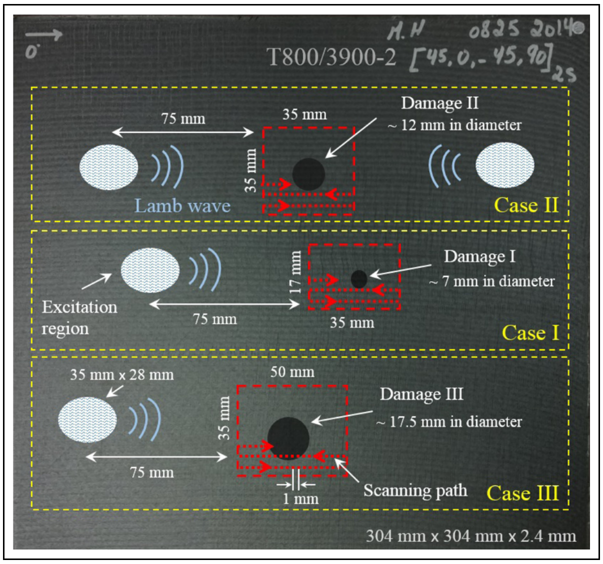

Figure 3. Composite laminate used in this study with different sizes of BVID. Three different cases (I, II, and III) represent the experimental setups for each damage imaging procedure.

where peak number $N = 5$, $S = 10$ is the signal intensity, $H(t)$ is the Heaviside step function, and f_c is the center frequency of the signal. The excitation signal was then amplified to a maximum voltage of 175 peak-to-peak voltage (Vpp) using the Krohn-Hite 7602 amplifier. An example of the five-cycle Hanning-windowed toneburst signal is presented in Figure 4.

The 1D time domain signal carried out from the LDV per measured point is fed to a MATLAB script that generates a 3D matrix for the scanned area. At the end of the scan, the 3D matrix could be sliced along the time axis and plotted as a snapshot of the propagating wavefield in the plate. A wave propagation video could also be generated by merging and presenting the snapshots in succession. The script also converts the measured spatial-time domain data into a frequency–wavenumber domain that helps in separating the forward propagating waves from the backward propagating waves due to any damage, discontinuity, or boundary in the inspected structure by applying the frequency–wavenumber filtering process discussed in "Theoretical background."

BVID imaging results

The A_0 Lamb wave mode is guided by the upper and lower surfaces of the composite plate, and when in contact with a discontinuity, part of the wave is scattered back, part is trapped within the damage, and the rest propagates through. The frequency–wavenumber (ω–k) filtering technique is therefore used to separate the forward propagating wave from any backward reflected waves along the wave path. The ω–k filtering technique used in the following study is applied to propagating waves in the regions of the three BVIDs with different dimensions. The first scanned region is a 35 mm $\times$ 17 mm area with 1 mm resolution including damage I, shown in Figure 3 as Case I. An ACT/LDV-scan for the following region is shown in Figure 5(a) and (b) at two different times (275 and 279 μs), where the generated A_0 mode is visible. An interaction between the propagating mode and the damage could be noticed inside the red-dashed region. Furthermore, the wavefield is also seen distorted to the right of the damaged region. When the ω–k filtering technique is applied to the detected wavefield, more information of the region's health could be extracted. The snapshots at 275 and 279 μs are also plotted for the backscattered waves in Figure 5(c) and (d). The backward waves from

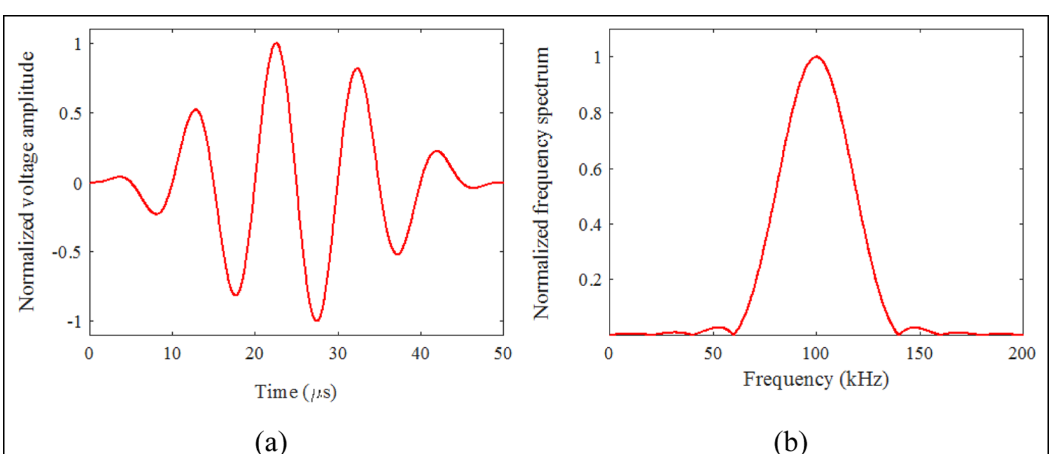

Figure 4. (a) Five-cycle Hanning-windowed toneburst input signal with a center frequency of 100 kHz and (b) its frequency spectrum.

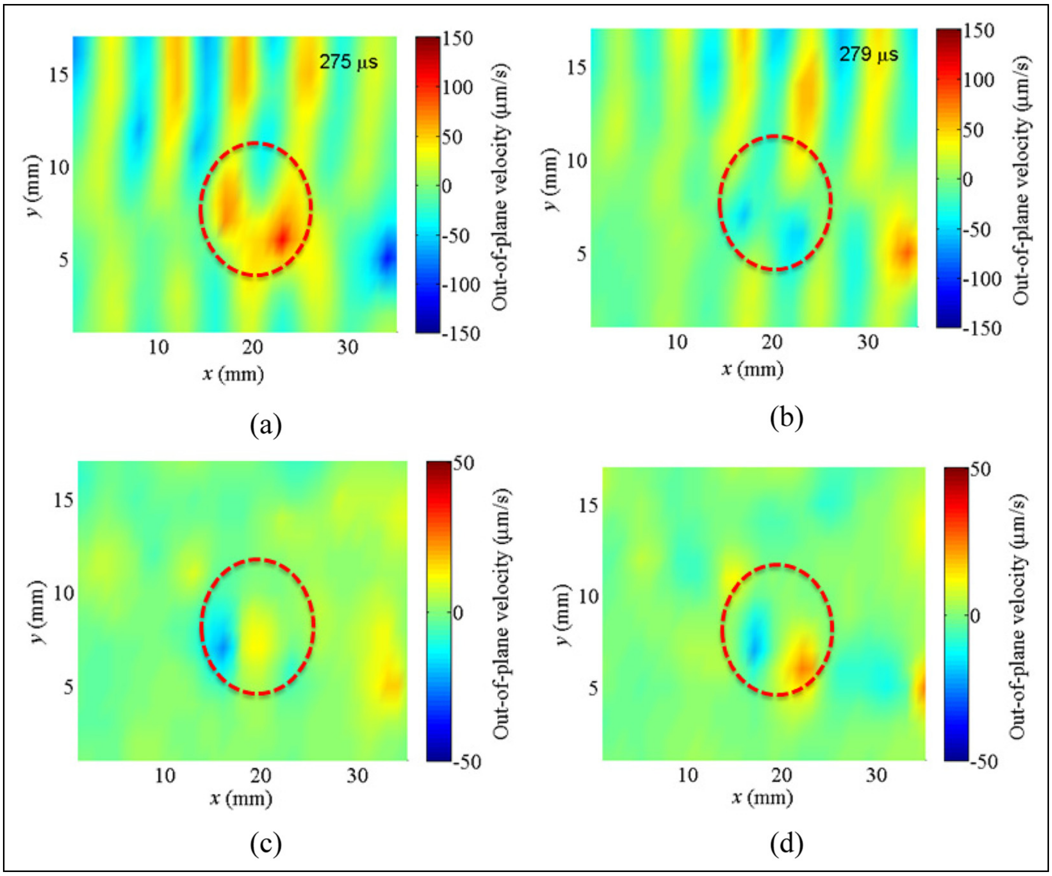

Figure 5. Incident A_0 mode propagating along the laminate captured at (a) 275 µs and (b) 279 µs with damage region in Case I represented with the red-dotted circle. The backward wavefield obtained using frequency–wavenumber filtering technique at (c) 275 µs and (d) 279 µs.

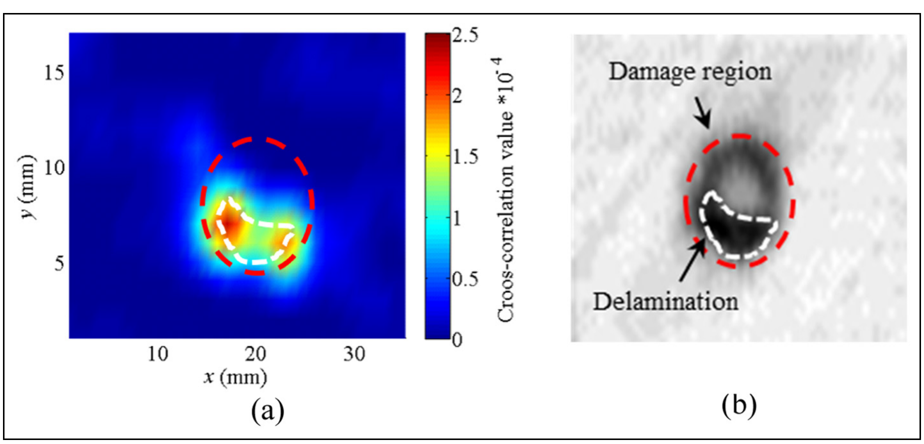

Figure 6. Case I: (a) Cumulative ZLCC image for damage I and (b) C-scan image.

the BVID are visible as the Lamb wave propagates through it.

Instead of using the backward wavefield in the time domain, a cross-correlation imaging between the forward wavefield and the backward wavefield is employed in the frequency domain as stated in section "Theoretical background." Figure 6(a) shows the generated image using ZLCC imaging condition technique where the whole region of the BVID is highlighted by the dashed-red region, and the C-scan image is

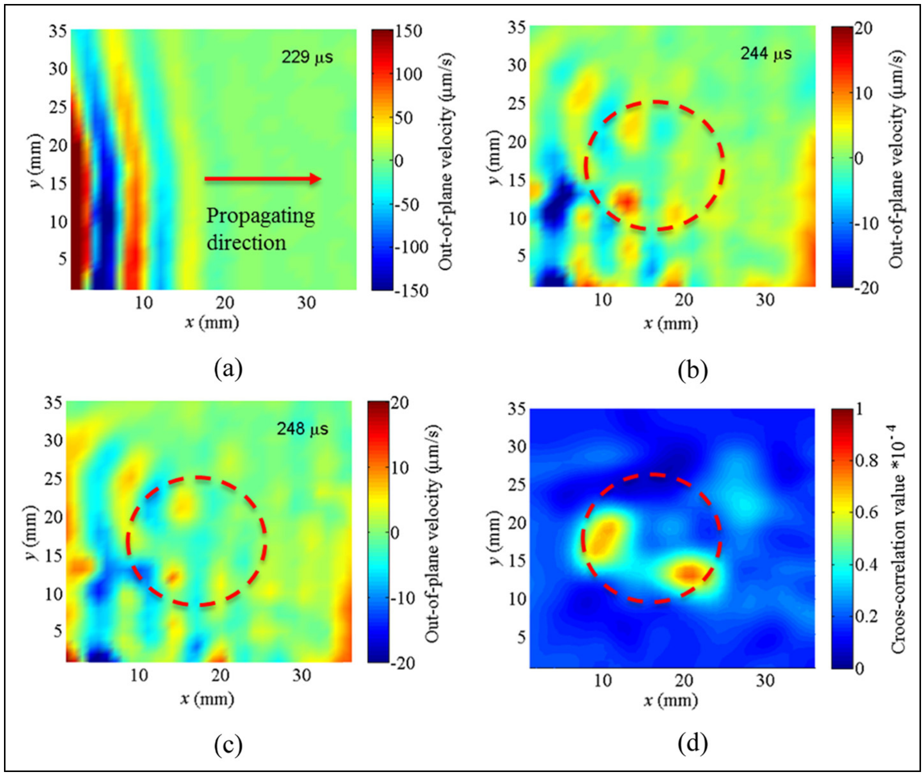

Figure 7. Case II: Incident A_0 mode propagating along the laminate captured at (a) 229 μs shows the incident wave direction (0°). The backward wavefield from damage II obtained using ω–k filtering technique (b) at 244 μs and (c) at 248 μs. (d) The ZLCC image for damage II when incident wave is traveling in the 0° direction.

provided in Figure 6(b). The delamination part of the damage is also displayed by the smaller dashed-white region in both figures. It is obvious that the resultant image mainly highlights the delaminated part with high ZLCC value representing a slightly larger region than the actual delamination.

Another 35 mm × 35 mm area including damage II is scanned by the LDV with a 1-mm resolution shown in Figure 3 as Case II. The region is first scanned with the ACT placed to the left of it and thus the excited wave propagates left to right as demonstrated in Figure 7(a). The backscattered waves from the damage II is extracted from the measured wavefield by applying the ω–k filter. Figure 7(b) and (c) displays the backward field from the damage at 275 and 279 μs, respectively, with the actual damage represented by a red-dashed region. Back propagating waves are noticed coming from inside and along the borders of circle. However, the damage is better observed when plotting the ZLCC value for the forward and backward wavefields as shown in Figure 7(d).

However, when comparing the ZLCC image to the C-scan, it is noticed that only part of the delamination is captured by this method. This may result from the interaction of the incident wave with the first delamination it encounters and thus any delamination behind that will be obstructed.

In order to visualize the whole damage, the area was then scanned again with the ACT placed to the right of this area as seen in Figure 3 (Case II), where the generated mode will travel from left to right as demonstrated in Figure 8(a). As the Lamb wave propagates through, waves are reflected back from any discontinuity as shown in Figure 8(b) and (c) and thus confirm the existence of a damage. The ZLCC imaging condition analysis was also applied, and the resultant values are plotted in Figure 8(d), where another delamination not captured by the first scan in Figure 7(d) is now noticed. In addition, the delamination to the left side of damage II is also hidden in this case because the incident wave is traveling from right to left.

The ZLCC images for damage II from both scans are then merged together, and the resultant is presented in Figure 9(a). When comparing the final image to the C-scan in Figure 9(b), a good agreement is noticed between the actual damaged area and the experimentally determined area. With the actual delaminations represented by white-dashed regions, the ZLCC image in Figure 9(a) does not highlight the whole delaminated regions, but it does provide good quantitative

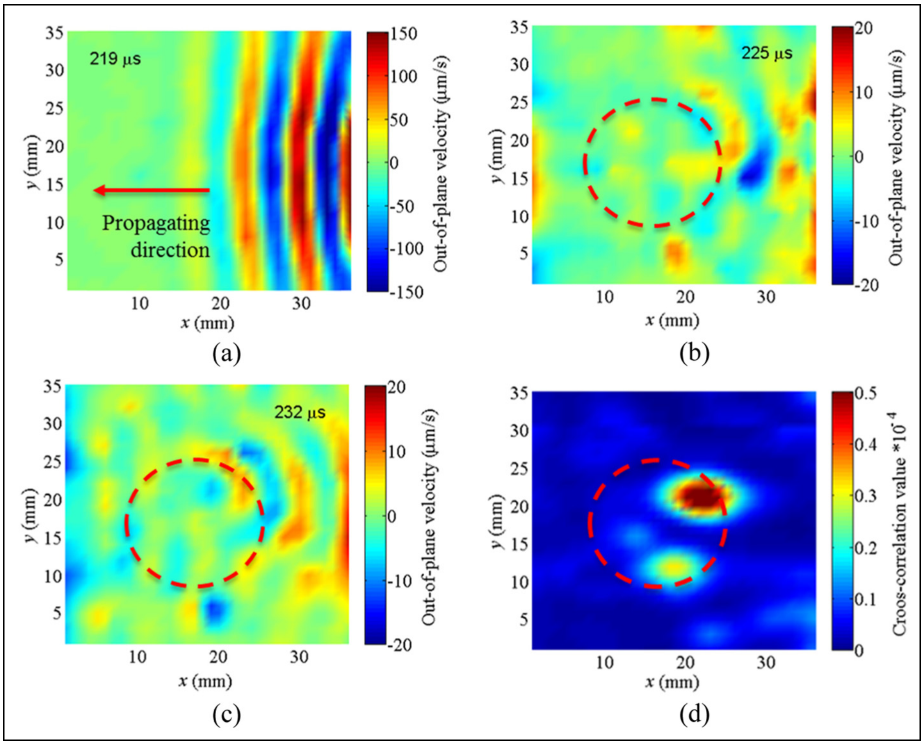

Figure 8. Case II: Incident A_0 mode propagating along the laminate captured at (a) 229 µs shows the incident wave direction ($-0°$). The backward wavefield from damage II obtained using ω–k filtering technique (b) at 225 µs and (c) at 232 µs. (d) The ZLCC image for damage II when incident wave is traveling in the $-0°$ direction.

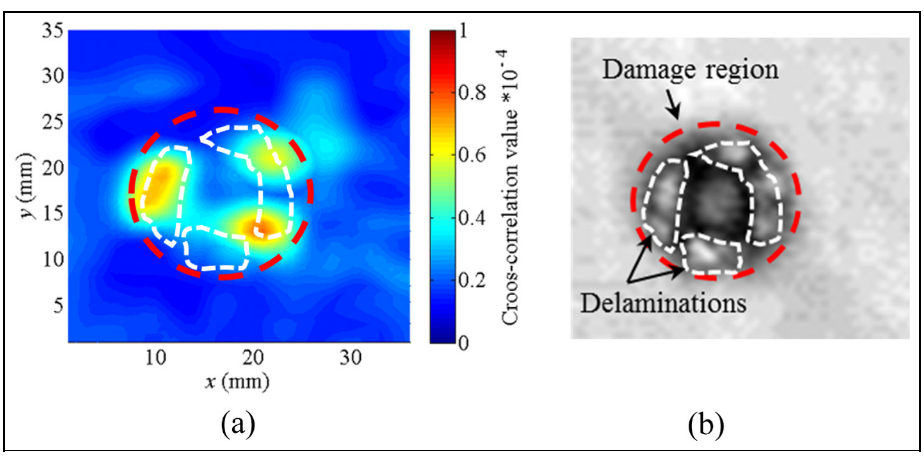

Figure 9. Case II: (a) Cumulative ZLCC image for damage II and (b) C-scan image.

information of the damaged regions. It is therefore found that with certain damages a double scan is needed in order to characterize the whole damage.

This criterion might be a limitation for the ZLCC imaging technique since the resultant values are dependent on the interaction of the backscattered and incident waves, when some of the incident waves are rendered by large delaminations.

Finally, the ZLCC imaging condition technique is also employed to generate an image for the third BVID, damage III, shown in Figure 3 as Case III. Figure 10 shows the images of propagating ultrasonic waves obtained over the inspection region, 50 mm × 35 mm, of the laminate at 244, 262, and 268 µs. The interaction between the incident wave and the damaged area (red-dashed region) is observed in Figure 10(b), where lower

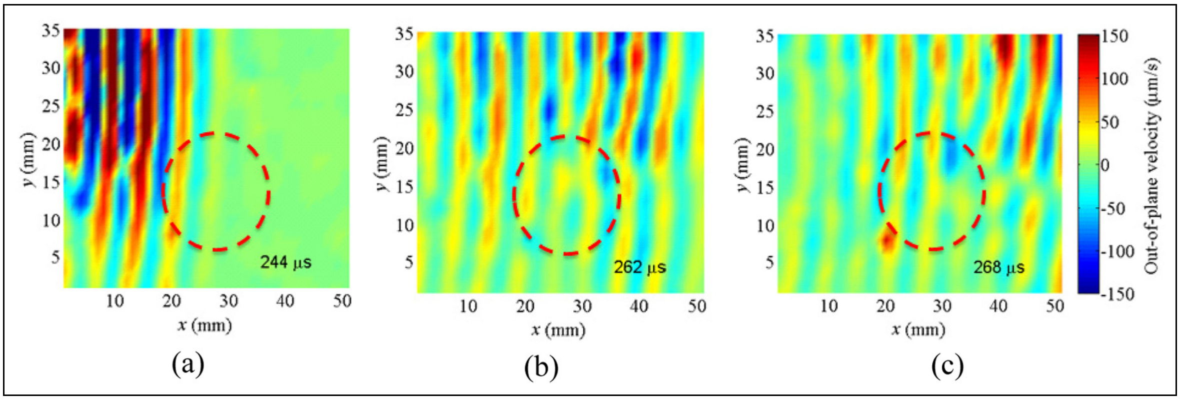

Figure 10. Case III: Incident A_0 mode propagating along the laminate captured at (a) 244 μs, (b) 262 μs, and (c) 268 μs shows the interaction of the wave with damage III represented by a red circle.

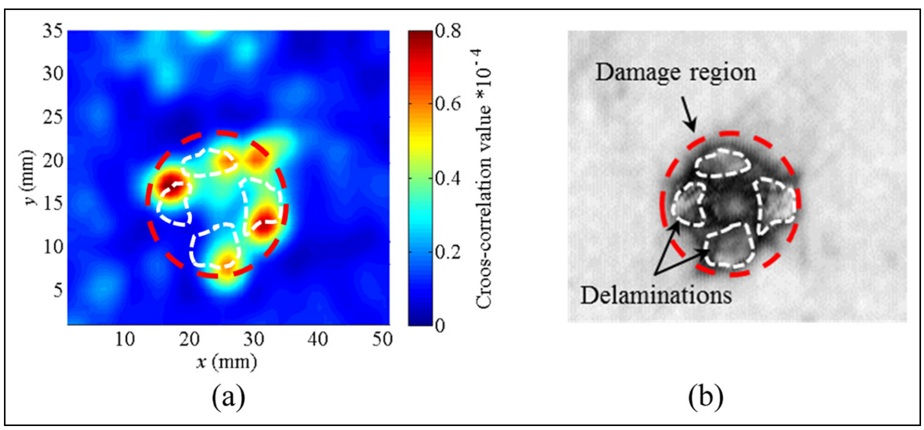

Figure 11. Case III: (a) Cumulative ZLCC image for damage III and (b) C-scan image.

amplitude of the wave is seen inside the circle with a slight change in the wave direction after the wave crosses the damage. Residual wave and trapped energy are also noticed in the damaged area after the ultrasonic wave has propagated through, as could be seen in Figure 10(c).

Because of multiple reflections and scattering near the damage and specifically around the delaminations, increased values of the ZLCC are expected in the regions of and around delaminations. As predicted, the ZLCC imaging condition plot for the forward against the backward wavefield in Figure 11(a) shows higher amplitudes inside and around damage III.

However, due to the complex shape of the damage and the presence of delaminations as well as an indentation area in the middle of the damage where the drop ball hit the plate, the experimental image shows much higher amplitudes at certain regions inside the damage which are good representations of the actual delaminations as shown in Figure 11(b). Mostly, the damage location and size are highlighted and thus enable the characterization of the BVID in the composite plate.

As noticed from the three studied cases, the LDV scanned areas were directly around the damaged regions in the plates, and it could be argued that the damage location is already known in this lab experiment which might not be the case on a part used out in the industry. However, the guided waves used in this study are known for their long distance propagation without losing much of the excited energy. Therefore, scanning the whole plate with the same special resolution will still present similar results but with our current setup it will take a much longer time. The LDV has a long standoff and could be set at a long distance away from the part of interest when only the ACT has to be close of the inspected region. In addition, upgrading to a 3D laser vibrometer provides the inspector with the in-plane velocities and displacements which are highly beneficial to further inspect the part and characterize the damage more precisely. Those features make the

ACT/LDV system with the ZLCC imaging method an excellent alternative over conventional ultrasound scanning methods.

Conclusion

Fundamental anti-symmetric (A_0) Lamb wave mode was used to investigate different BVIDs in a T800/3900-2 $(45/0/\text{-}45/90)_{2S}$ laminate. The A_0 mode was generated using a fully non-contact air-coupled ultrasonic transducer (ACT) placed 80 mm away from the inspected surface of the thin composite and detected at some distance away using a LDV by measuring the out-of-plane velocity of the composite surface along a scanning grid. A ZLCC imaging condition technique in the frequency domain was applied by cross-correlating the forward and backward propagating wavefields separated from the actual measured wavefield using frequency–wavenumber (ω–k) filtering technique. The hybrid non-contact ACT/LDV system and the ZLCC imaging condition technique have been verified in three experimental case studies investigating their capability in detecting and sizing different delaminations with different sizes and at different locations in a flat composite plate. However, this method has not been thoroughly tested on curved panels or more complex shaped parts. Initial investigation from a curved panel has shown promising results for the air-coupled and laser system which will be further analyzed and presented in another publication.

The experimental ZLCC images highlight the three damaged regions with higher ZLCC values in and around the delaminations compared to other parts of the inspected region of the composite. However, it was found that certain smaller delaminations could not be readily detected. This is a result of the generated wavefield interacting with a large delamination overwhelming over that from any smaller ones. It is concluded that with the current setup it is more beneficial to scan the region of interest with the incident wave propagating from at least two locations to capture the full image of the delaminated region. Superimposing the resultant images will give a good approximated damaged area. It is also noted that using a 3D LDV which captures the in-plane and out-of-plane displacements and velocities will help to overcome the issue of multi-scanning faced in this experiment.

The experimental investigation for all three BVIDs has shown a good correlation between the ZLCC imaging condition and C-scan images. In summary, this work illustrates the feasibility of using the hybrid system and the guided wave ZLCC imaging condition in characterizing BVIDs in CFRP panels. This system is a complete non-contact scanning system that could be easily used in different working conditions and without altering or disassembling the inspected parts. The LDV also provides a large standoff distance from the part that makes it more feasible to be used for automated inspections of large structures like airplanes, wind turbines, and bridges.

Acknowledgements

Mr MS Harb would like to acknowledge the financial support provided by the Graduate Research Assistantship (GRA) from National Institute of Aerospace through NASA Langley Research Center, and he would also like to gratefully acknowledge Mr Tyler Hudson for helping in specimen preparation and Mr Wade Jackson for helping in impacting and C-scanning the composite at NASA Langley Research Center.

Declaration of Conflicting Interests

The author(s) declared no potential conflicts of interest with respect to the research, authorship, and/or publication of this article.

Funding

The author(s) received no financial support for the research, authorship, and/or publication of this article.

References

1. Green RE. Non-contact ultrasonic techniques. *Ultrasonics* 2004; 42: 9–16.
2. Chimenti DE. Review of air-coupled ultrasonic materials characterization. *Ultrasonics* 2014; 54: 1804–1816.
3. Kazys R, Demcenko A, Zukauskas E, et al. Air-coupled ultrasonic investigation of multi-layered composite materials. *Ultrasonics* 2006; 44: e819–e822.
4. Raisutis R, Kazys R, Zukauskas E, et al. Ultrasonic air-coupled testing of square-shape CFRP composite rods by means of guided waves. *NDT&E Int* 2011; 44: 645–654.
5. Ramadas C, Janardhan Padiyar M, Balasubramaniam K, et al. Delamination size detection using time of flight of antisymmetric (A_0) and mode converted A_0 mode of guided Lamb waves. *J Intel Mat Syst Str* 2010; 21: 817–825.
6. Ramadas C, Balasubramaniam K, Joshi M, et al. Interaction of Lamb wave mode (A_0) with structural discontinuity and generation of "Turning modes" in a T-joint. *Ultrasonics* 2011; 51: 586–595.
7. Harb MS and Yuan FG. A rapid, fully non-contact, hybrid system for generating Lamb wave dispersion curve. *Ultrasonics* 2015; 61: 62–70.
8. Harb MS and Yuan FG. Damage imaging using non-contact air-coupled transducer/laser Doppler vibrometer system. *Struct Health Monit* 2016; 15(2): 193–203.
9. Ruzzene M. Frequency-wavenumber domain filtering for improved damage visualization. *Smart Mater Struct* 2007; 16: 2116–2129.
10. Michaels TE, Michaels JE and Ruzzene M. Frequency—wavenumber domain analysis of guided wavefields. *Ultrasonics* 2011; 51: 452–466.

11. Alleyne D and Cawley P. A two-dimensional Fourier transform method for the measurement of propagating multimode signals. *J Acoust Soc Am* 1991; 89: 1159–1168.
12. Tian Z and Yu L. Lamb wave frequency-wavenumber analysis and decomposition. *J Intel Mat Syst Str* 2014; 25(9): 1107–1123.
13. Yu L and Tian Z. Lamb wave structural health monitoring using a hybrid PZT-laser vibrometer approach. *Struct Health Monit* 2013; 12: 469–483.
14. Glushkov E, Glushkova N, Golub M, et al. Wave energy trapping and localization in a plate with a delamination. *Smart Mater Struct* 2012; 21: 125001–125012.
15. Lee J-R, Chia CC, Shin HJ, et al. Laser ultrasonic propagation imaging method in the frequency domain based on wavelet transformation. *Opt Laser Eng* 2011; 49: 167–175.
16. Sohn H, Dutta D, Yang JY, et al. Automated detection of delamination and disbond from wavefield images obtained using a scanning laser vibrometer. *Smart Mater Struct* 2011; 20: 045017 (10 pp.).
17. An YK, Park B and Sohn H. Complete noncontact laser ultrasonic imaging for automated crack visualization in a plate. *Smart Mater Struct* 2013; 22: 025022 (10 pp.).
18. Zhu R, Huang GL and Yuan FG. Fast damage imaging using the time-reversal technique in the frequency-wavenumber domain. *Smart Mater Struct* 2013; 22: 075028 (11 pp.).
19. Sava P and Vlad I. Wide-azimuth angle gathers for wave-equation migration. *Geophysics* 2011; 76(3): S131–S141.
20. Chang W and McMechan G. Reverse-time migration of offset vertical seismic profiling data using the excitation-time imaging condition. *Geophysics* 1986; 51: 67–84.
21. Claerbout J. Toward a unified theory of reflector mapping. *Geophysics* 1971; 36(4): 67–81.
22. Jitsumori A, Inoue S, Maekawa T, et al. Generation of Lamb wave using linear array probe and its application for flaw detection. *Jpn J Appl Phys* 1986; 25: 200–202.